Thin-Sample Measurements and Error Analysis of High-Temperature Coaxial Dielectric Probes

Shane Bringhurst, *Member, IEEE,* Magdy F. Iskander, *Fellow, IEEE,* and Mikel J White

***Abstract*— A metallized-ceramic probe has been designed for high-temperature broad-band dielectric properties measurements. The probe has been used to make complex dielectric properties measurements over the complete frequency band from 500 MHz to 3 GHz, and up to temperatures as high as 1000 °C. In this paper, we investigate new aspects of the development and utilization of this high-temperature dielectric probe. The first aspect is related to the results of an uncertainty analysis which was performed to quantify the errors due to the differential thermal expansion between the inner and outer conductors of metal coaxial probes. In this case, a two-dimensional (2-D) cylindrical finite-difference time-domain (FDTD) code was developed and used for this analysis. The obtained results were compared and shown to be in good agreement with error-analysis data based on analytical solutions for the special case when an air gap exists between the probe and the material under test. Additional new error-analysis results show that differential thermal expansions and rough surfaces cause considerable errors in these measurements, and the use of probes of small differential thermal expansions, such as the developed metallized-ceramic probe, is essential for obtaining accurate results. We also used FDTD numerical simulations to help investigate the use of this probe for the nondestructive complex-permittivity measurements of electrically "thin" samples. It is shown that by backing the material under test with a standard material of known dielectric constant, such as air or metal, the complex permittivity of thin samples can be accurately measured. The other new development is related to the use of the developed metallized-ceramic probe to measure the dielectric properties of thin samples at high temperature and over a broad frequency band. With the developed knowledge from the error analysis, and the new FDTD code for thin-sample measurements, the metallized-ceramic probe was used to measure dielectric properties of thin Al_2O_3 and sapphire samples for temperatures up to 1000 °C. This measurement method has important applications in the on-line characterization of semiconductor wafers. Results from the high-temperature thin-sample measurements and the uncertainty analysis are presented.**

***Index Terms*—Complex permittivity, dielectric constant, dielectric probe, error analysis, FDTD, thin-sample measurement.**

I. Introduction

OPEN-ENDED coaxial probes have been used for dielectric properties measurements for several years [1]–[5]. The attractiveness of the open-ended coaxial-probe measurement procedure has been in the relative ease of the measurement procedure, the broad-band measurement capabilities, and the possible on-line use of the probe. The open-ended probe basically consists of a truncated section of a coaxial line, with an optional extension of a ground plane. The probe is connected to a vector network analyzer (HP8510) through a coaxial cable. The sample under test is placed flush with the probe and the value of the complex permittivity is then determined from the measurement of the input impedance of the probe. Several formulas are available for relating the measured input impedance to the complex permittivity of the material under test. Even a commercial software package is available from Hewlett-Packard for making these measurements [6].

However, none of the available metal probes can be used to provide accurate results at temperatures as high as 1000 °C. This is due to problems with the differential thermal expansion of the inner and outer conductors in metal probes. Even the use of metals with small thermal-expansion coefficients, such as kovar, has resulted in limited success in providing reasonable results for temperatures up to 600 °C. At higher temperatures, the differential thermal expansion between the inner and outer conductors of the kovar probe significantly increased and, hence, affected the accuracy of the measurements [7]. The metallized-ceramic probe solved the differential thermal-expansion problem and made it possible to perform high-temperature dielectric properties measurements with an open-ended coaxial probe [1].

The use of open-ended coaxial probes has also been recently extended to the measurement of the dielectric properties of thin samples [8], [9]. This has not been done in the past due to the requirement of satisfying the infinite sample criteria in the calculation procedure. In this paper, we will describe the use of the metallized-ceramic probe together with the utilization of the FDTD calculation procedure to extend dielectric-measurement capabilities to thin samples. The thin-sample dielectric-measurements calculation procedure, together with gained understanding from the uncertainty analysis of the high-temperature measurements, were then used to measure dielectric properties of materials of significant interest to the semiconductor industry. Results of thin-samples measurements on alumina and sapphire in the frequency band from 0.5 to 3.0 GHz, and for temperatures up to 1000 °C will be presented.

A. FDTD Code Development

Since air gaps that exist in coaxial probe measurements are generally on the order of a fraction of a millimeter, it was necessary to create an FDTD code capable of modeling

Manuscript received August 13, 1996; revised August 22, 1997.

S. Bringhurst was with the Electrical Engineering Department, University of Utah, Salt Lake City, UT 84112 USA. He is now with Texas Instruments, Incorporated, McKinney, TX 75070 USA.

M. F. Iskander is with the Electrical Engineering Department, University of Utah, Salt Lake City, UT 84112 USA.

M. J White was with the Electrical Engineering Department, University of Utah, Salt Lake City, UT 84112 USA. He is now with Texas Instruments, Incorporated, Dallas, TX 75243 USA.

Publisher Item Identifier S 0018-9480(97)08240-9.

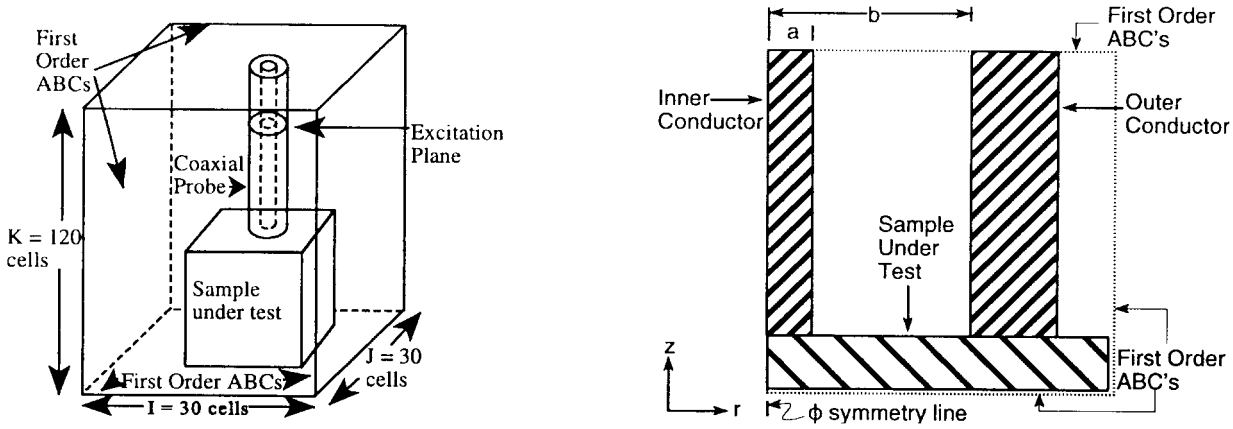

Fig. 1. Computational domain and probe geometry for both a (a) 3-D and (b) 2-D model.

extremely small cell sizes, and at the same time fitting within available computational resources. To numerically model an air gap on the order of 0.1 mm, a typical three-dimensional (3-D) FDTD model of $30 \times 30 \times 120$ mm^3 would be on the order of 100 million cells. Such a large model is far beyond available computational resources. For this purpose, a cylindrical two-dimensional (2-D) FDTD code was developed which makes use of the Φ-symmetry in coaxial probes, and the symmetry around the center line of the probe.

Fig. 1 shows the computational domain and the probe geometry for both a 2-D and 3-D model. First-order absorbing boundaries are placed around the probe to limit the computational domain and increase the computational efficiency. The use of simple first-order radiation boundaries is justified due to the limited radiation from the open-ended probe. The computational domain was made two to ten cells larger than the sample dimensions to avoid possible computational errors.

The excitation plane is placed inside the coaxial probe about three-fourths of a wavelength from the open end of the probe. A forward moving (toward the measurement end) TEM wave is launched at the excitation plane, and the field distributions in both the sample and the coaxial probe are calculated using a routine Yee cell procedure [10]. "History" test points were located in the coaxial probe and in the sample to ensure convergence of the solution. The input impedance of the material under test was obtained by calculating the potential difference between the coaxial conductors, and the current on the center conductor, using (1) and (2) [1], [11]:

$$\int \overline{\mathbf{E}} \cdot \overline{dl} = V \tag{1}$$

$$\oint \overline{\mathbf{H}} \cdot \overline{dl} = I. \tag{2}$$

With the cylindrical 2-D FDTD code using a cell size of 0.1 mm, the resulting model was only 180 000 cells, which is certainly manageable and computationally efficient.

B. Uncertainty Analysis of High-Temperature Dielectric Properties Measurements

It is of considerable interest to quantify possible errors that may result from the differential thermal expansion between the inner and outer conductors in open-ended probes. This differential thermal expansion in metal probes may be caused by the outer conductor heating faster during the heating cycle, and cooling faster during the cooling cycle in a typical high-temperature dielectric properties measurement. During the heating cycle, therefore, the outer conductor expands faster than the inner conductor, causing air gaps between the inner conductor and the material under test. On the other hand, during the cooling cycle the outer conductor shrinks faster than the inner conductors, which causes an air gap between the outer conductor and the material being measured. It is of interest to quantify the errors in dielectric properties measurements as a result of the differential thermal expansion in metal probes.

The equation for calculating the length of the gap between the inner and outer conductors (ΔT) due to thermal expansion is given by [12] as follows:

$$\delta_T = \alpha(\Delta T)L \tag{3}$$

where α is the coefficient of thermal expansion, ΔT is the temperature difference between the inner and outer conductors, and L is the length of the probe at room temperature. The coefficient of thermal expansion for stainless steel is 19.1 ($10^{-6}/°$C) [13], therefore, a typical metal probe (12 cm in length) made of stainless steel would have a 0.1-mm air gap between the inner and outer conductors for only a 43.6 °C temperature difference. This type of heat differential is certainly possible when the probe is heated to temperatures as high as 800 °C–1000 °C, which are common for ceramic sintering. Therefore, since the differential thermal expansion between the inner and outer conductors is generally on the order of a fraction of a millimeter, it was necessary to create the previously mentioned FDTD code which is capable of modeling extremely small cell sizes and at the same time fitting within available computational resources.

Papers have been recently published to quantify errors due to air gaps between the coaxial probe and the surface of the material under test [1], [14]. In this paper, focus will be placed on quantifying errors due to air gaps which may result from the differential thermal expansion between the inner and outer

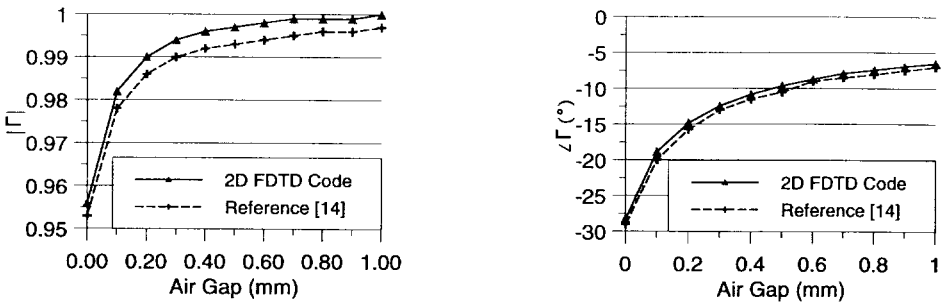

(a) (b)

Fig. 2. Calculated FDTD results versus analytical results of the reflection coefficient (a) magnitude and (b) phase. Results are for a sample with $\epsilon_r^* = 10 - j\,1$ measured with a probe with dimensions $a = 1.9$ mm and $b = 7$ mm at 1 GHz. Probe has filler material of $\epsilon_r' = 2.54$.

conductors, and also due to surface roughness of the sample under test.

To verify the accuracy of the cylindrical 2-D FDTD code, the input impedance of the probe was calculated as a function of the air-gap width and the results were compared with analytical results recently published in [14]. The model consisted of a probe with inner conductor of radius 1.9 mm and outer conductor of radius 7 mm. The probe was filled with a filler material of dielectric constant $\epsilon_r' = 2.54$, and the sample under test had complex-permittivity value of $\epsilon_r^* = 10 - j1$. The measurements were done at 1 GHz. A uniform air gap of 0 to 1 mm (in increments of 0.1 mm) between the probe and the sample under test was modeled. The results of the reflection coefficient as measured with the FDTD modeling versus analytical results available in [14] are shown in Fig. 2. The magnitude of the reflection coefficient is shown in Fig. 2(a), and the phase is shown in Fig. 2(b). After calculating the input impedance, the reflection coefficient Γ_L was calculated using (4):

$$\Gamma_L = \frac{Z_L - Z_0}{Z_L + Z_0} \tag{4}$$

where Z_L is the input impedance of the probe and Z_0 is the characteristic impedance of the coaxial line.

Fig. 2 shows a high degree of accuracy between the analytical results [14] and the developed 2-D cylindrical FDTD code. It should be noted that the air gaps due to differential thermal expansion are different from the air gaps analyzed using the analytical procedure [14]. The analytical results are for uniform air gaps between the probe and the surface of the sample. The air gaps of interest to our study are between just the inner or outer conductor and the sample. A series of simulations were modeled to quantify how air gaps affect the obtained dielectric results for different types of materials, and at different frequencies. Two typical materials that are often used in microwave sintering were modeled. This includes low-loss material Al_2O_3 with complex permittivity $\epsilon_r^* = 9.93 - j0.002$, and high-loss material SiC with complex permittivity $\epsilon_r^* = 29.0 - j6.6$.

1) Air-Gap Effects for Different Materials: When simulating the effects of differential thermal expansion, the probe was first modeled flush against the material under test, and then an air gap of 0.1 to 1 mm (in increments of 0.1 mm) between the inner conductor and the material under test was modeled. The same procedure was repeated, but with the air gap between the outer conductor and the material under test. Fig. 3(a) and (b) show the errors in the measured input impedance due to the differential thermal expansion during the heating cycle, which results in an air gap between the inner conductor and the material under test for both a high-loss material (SiC) and a low-loss material (Al_2O_3). Fig. 3(c) and (d) show the corresponding errors in ϵ' and ϵ'' of these samples.

Fig. 4(a) and (b) shows the errors in the measured input impedance due to the differential thermal expansion during the cooling cycle, which results in an air gap between the outer conductor and the material under test, for both high-loss (SiC) and low-loss (Al_2O_3) materials. Corresponding errors in ϵ' and ϵ'' for these samples are shown in Fig. 4(c) and (d). The results shown in Fig. 4 were calculated at 3 GHz.

From Figs. 3 and 4, it may be seen that a 0.1-mm gap, particularly between the center conductor and the material under test, may result in a significant error in the input impedance and the complex-permittivity values. It is interesting to note that an air gap, on the order of 0.1 mm, between the inner conductor and the material under test can cause an error in the input impedance of 170%. This is the kind of gap that will exist in a metal probe when the temperature difference between the inner and outer conductors is less than 50 °C. Even in a low-loss material there can be errors in the input impedance as high as 50% and a corresponding error in ϵ' as high as 43%. Use of metal probes for these high-temperature dielectric properties measurements is, therefore, highly undesirable. Furthermore, it may be observed from Figs. 3 and 4 that errors in the input impedance and complex permittivity are much larger for an air gap between the inner conductor and the material under test. This stands to reason since the inner conductor carries the current and more of the electromagnetic fields are concentrated between the center conductor and the sample.

This may be further verified by viewing the resultant electric field $|E|^2$ inside the probe and in the sample when air gaps are present. Fig. 5 shows a comparison between a probe that is flush with an Al_2O_3 sample [Fig. 5(a)] and a probe that has an air gap between the inner conductor and an Al_2O_3 sample [Fig. 5(b)]. Fig. 6 shows a comparison between a probe that is flush with an Al_2O_3 sample [Fig. 6(a)] and a probe that has an air gap between the outer conductor and

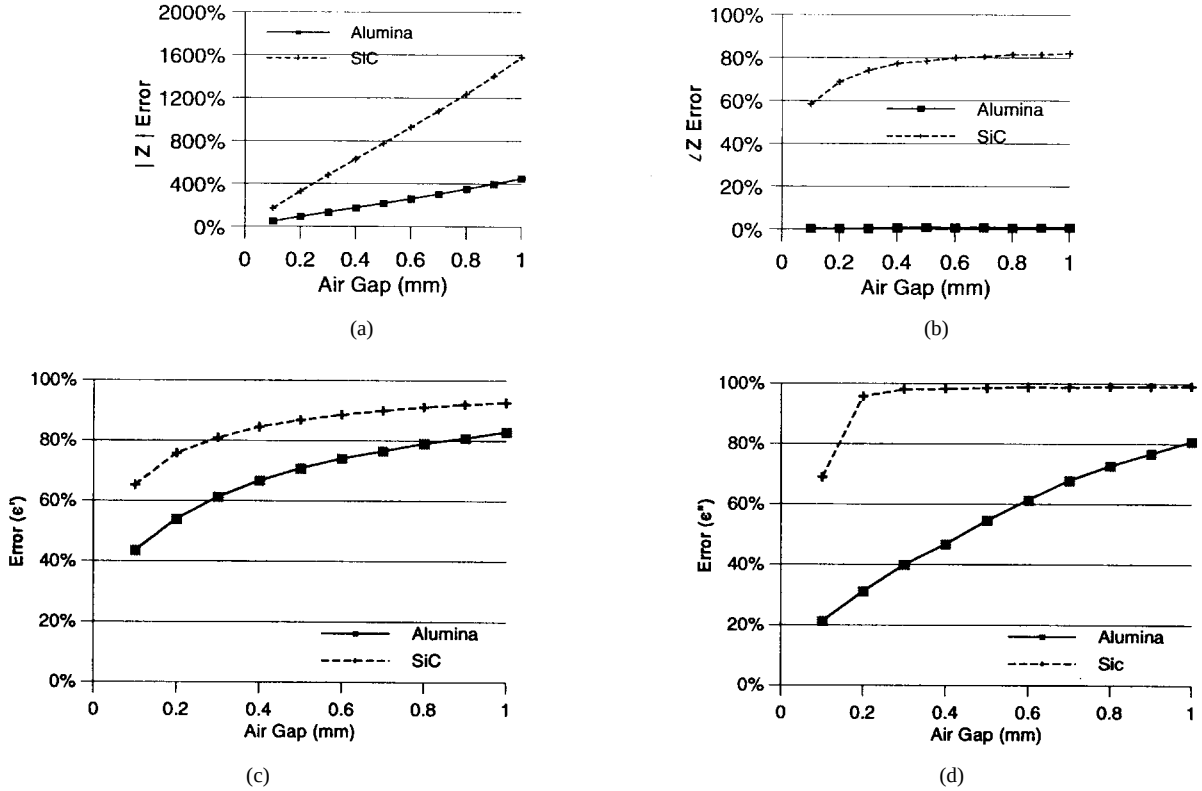

Fig. 3. Percent error in the input impedance and dielectric properties when air gaps are between the inner conductor and the sample under test. (a) Impedance magnitude, (b) impedance phase, (c) ϵ', and (d) ϵ'' errors for both SiC and Al_2O_3. Air gaps between the inner conductor and the material under test result from the differential thermal expansion in metal probes during the heating cycle. Calculations were made at 3 GHz.

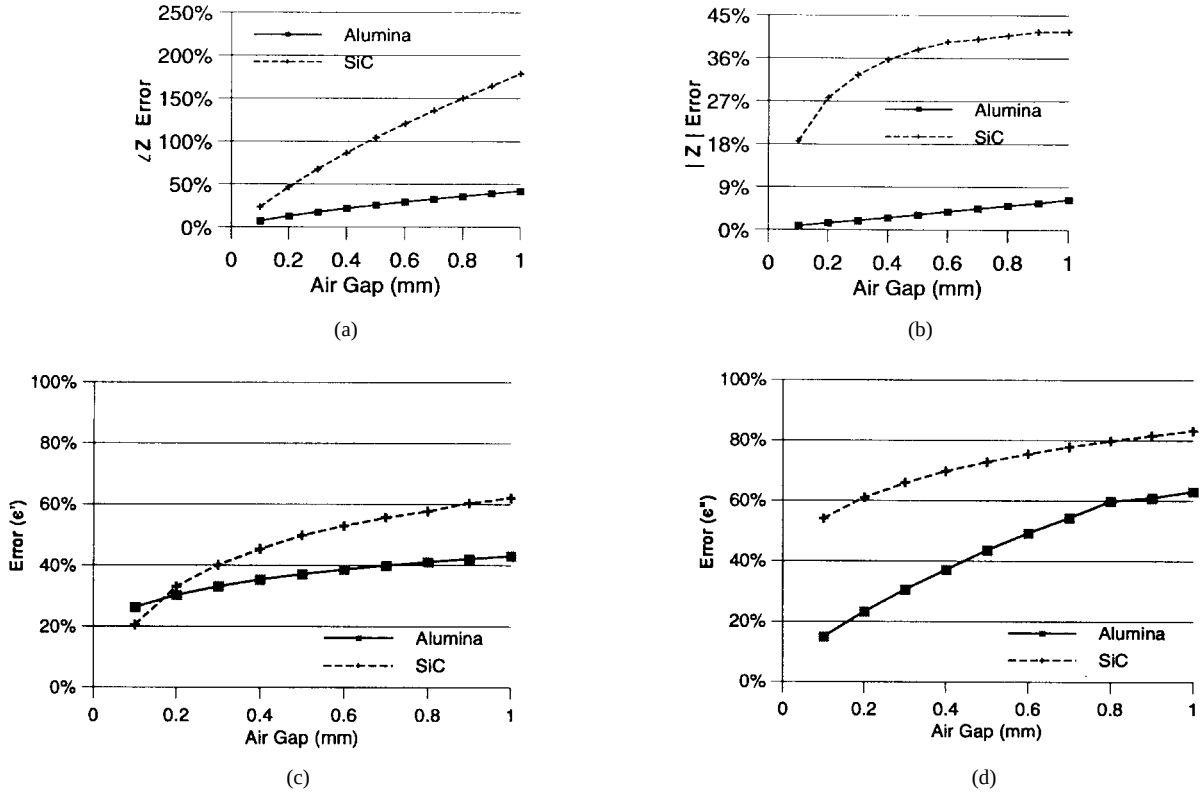

Fig. 4. Percent error in the input impedance and dielectric properties due to air gaps between the outer conductor and the sample under test. (a) Errors in impedance magnitude, (b) errors in impedance phase, (c) ϵ', and (d) ϵ'' errors for both SiC and Al_2O_3. Air gaps between the outer conductor and the material under test result from the differential thermal expansion in metal probes during the cooling cycle. Calculations were made at 3 GHz.

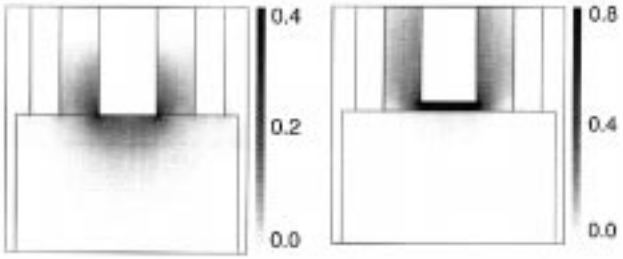

(a) (b)

Fig. 5. Resultant electric field $|E|^2$ as calculated with FDTD for (a) no air gap between the probe and an Al_2O_3 sample, and (b) an air gap between the inner conductor of the probe and an Al_2O_3 sample.

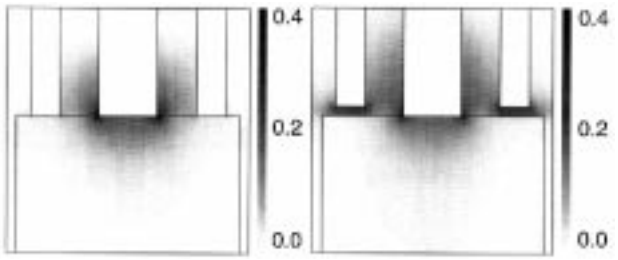

(a) (b)

Fig. 6. Resultant electric field $|E|^2$ as calculated with FDTD for (a) no air gap between the probe and an Al_2O_3 sample, and (b) an air gap between the outer conductor of the probe and an Al_2O_3 sample.

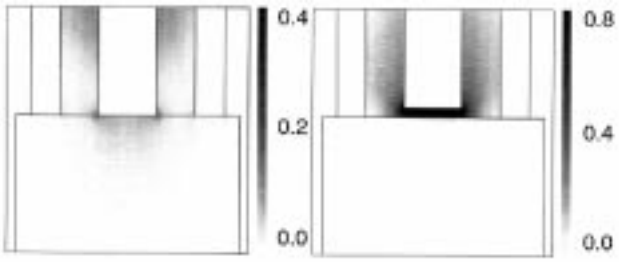

(a) (b)

Fig. 7. Resultant electric field $|E|^2$ as calculated with FDTD for (a) no air gap between the probe and an SiC sample, and (b) an air gap between the inner conductor of the probe and an SiC sample.

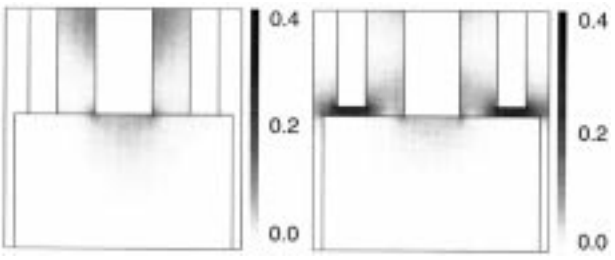

(a) (b)

Fig. 8. Resultant electric field $|E|^2$ as calculated with FDTD for (a) no air gap between the probe and an SiC sample, and (b) an air gap between the outer conductor of the probe and an SiC sample.

an Al_2O_3 sample [Fig. 6(b)]. These FDTD results clearly demonstrate the enhanced sensitivity to air gaps between the center conductor and the sample because of the larger fields present in this case.

From Figs. 3 and 4, it may also be observed that errors are much larger for the high-loss material than for the low-loss material. Fig. 7 shows a comparison between a probe that is flush with an SiC sample [Fig. 7(a)], and a probe that has an air gap between the inner conductor and an SiC sample [Fig. 7(b)]. Fig. 8 shows a comparison between a probe that is flush with an SiC sample [Fig. 8(a)] and a probe that has an air gap between the outer conductor and an SiC sample [Fig. 8(b)].

From Figs. 7 and 8, it may be seen that when there is no air gap between the probe and an SiC sample that there are very little fields present at the surface of the sample. This is because the dielectric properties of SiC are sufficiently high that the sample almost appears as a short. Therefore, when a gap appears between either the inner or outer conductor and the SiC sample, there is a much greater distortion of the fields than if the sample were an Al_2O_3 sample or other type of low complex-permittivity material. For this reason the errors are greater when air gaps are present with high-loss samples than with low-loss materials.

2) Frequency Effects on Air Gaps: Fig. 9 shows the frequency dependence of errors in ϵ' measurements due to air gaps when the probe is used to test a high-loss material (e.g., SiC). Fig. 9(a) shows the percent error due to an air gap between the inner conductor and the material under test at the three frequencies 915 MHz, 2 GHz, and 3 GHz, while Fig. 9(b) shows the percent error in ϵ' due to an air gap between the outer conductor and the material under test at the same three frequencies. Fig. 10(a) shows the error due to an air gap between the inner conductor and a low-loss material under test while Fig. 10(b) shows the errors when the air gap is between the outer conductor and the low-loss material (Al_2O_3) under test.

From the results shown in Figs. 9 and 10, it appears that frequency has more effect on errors for high-loss materials than it does on low-loss materials. Frequency effects were small when measuring the properties of both Al_2O_3 and SiC, although there was slightly more variation between the frequency results for the SiC. The observed relative insensitivity of the calculated errors at different frequencies may be justified in terms of the relatively small sizes of these gaps compared to the wavelength at the reported frequencies. Therefore, larger frequency effects may be expected at higher frequencies, which are beyond the scope of the developed probe.

3) Surface Roughness Effects: Another analysis was done to examine how roughness would affect the measured input impedance of the samples under test. For this analysis, extremely small discontinuities or aberrations were numerically simulated on the surface of the sample under test and compared with the case of a smooth-surface simulation. Several simulations were done with various patterns of surface roughness to determine general trends in errors caused by the surface roughness. The obtained results suggested that the magnitude of errors strongly depends on the location of the aberration with respect to the probe. Therefore, a set of FDTD simulations

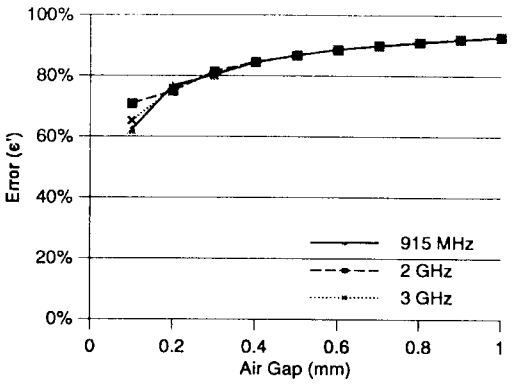

(a)

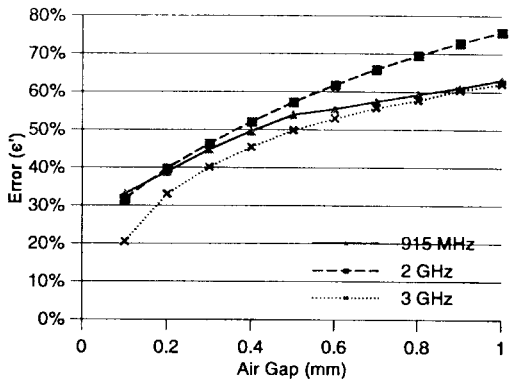

(b)

Fig. 9. Percent error in ϵ' measurements of SiC at three different frequencies: 915 MHz, 2 GHz, and 3 GHz. Errors are due to an air gap between (a) the inner conductor and the material under test and (b) the outer conductor and the material under test. Gaps at the inner conductor result from the differential thermal expansion in metal probes during the heating cycle while gaps at the outer conductor result from differential thermal expansion during the cooling cycle.

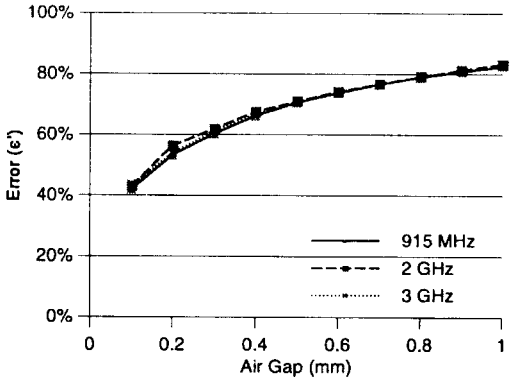

(a)

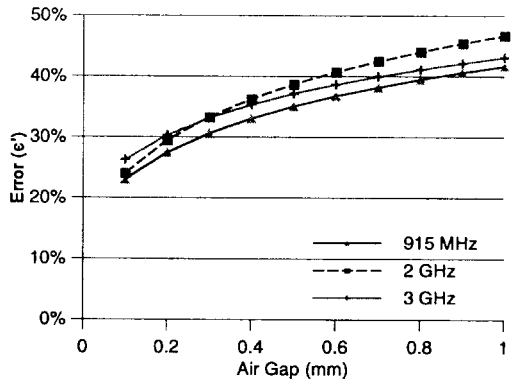

(b)

Fig. 10. Percent error in ϵ' measurements of Al_2O_3 at three different frequencies: 915 MHz, 2 GHz, and 3 GHz. Errors are due to an air gap between (a) the inner conductor and the material under test and (b) the outer conductor and the material under test.

were undertaken by placing just one aberration on the surface of the sample, but at various locations with regards to the probe. The surface aberrations were placed in six different spots, as illustrated in Fig. 11. The aberrations were located directly below the center of the inner conductor, below the edge of the inner conductor, right in the middle of the inner and outer conductors, below the inside edge of the outer conductor, below the center of the outer conductor, and below the outside edge of the outer conductor. The aberrations were also made to be two different sizes: $0.1 \times 0.1 \times 0.1$ mm^3, and $0.2 \times 0.2 \times 0.2$ mm^3. However, these aberrations were simulated using the 2-D FDTD code and, hence, cylindrical symmetry was assumed. In other words, each aberration was represented by a circular ring of 0.1×0.1 mm^2 and 0.2×0.2 mm^2 cross-sectional dimensions. The impedance calculations were made and compared to the test case when there was no surface roughness. Tests were once again conducted on both a high-loss material (SiC) and on a low-loss material (Al_2O_3). Tables I and II show the FDTD results of the effect of surface roughness on the input impedance values for both 0.1×0.1 mm^2 and 0.2×0.2 mm^2 aberrations, respectively. Because of the 2-D nature of these calculations, the results presented in Tables I and II may be considered as upper limits to expected errors.

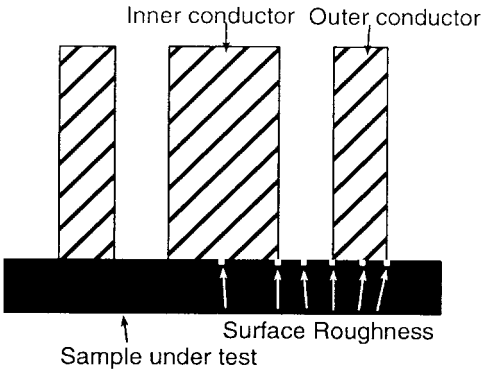

Fig. 11. Placement of surface roughness with respect to dielectric probe. FDTD calculations were used to study the separate effect of each of these aberrations on the calculations of the input impedance.

The results show that the surface roughness has to be on the edge of one of the conductors to produce a significant effect. Even then the effect on the magnitude of the input impedance is negligible unless the surface roughness is on the edge of the

TABLE I
PERCENTAGE CHANGE IN THE MAGNITUDE AND PHASE OF THE INPUT IMPEDANCE DUE TO SURFACE ROUGHNESS (ON THE ORDER OF 0.1 × 0.1 MM^2) OF A LOW-LOSS MATERIAL Al_2O_3 AND A HIGH-LOSS MATERIAL SiC

Placement of surface roughness aberration:	Al_2O_3		SiC	
	Magnitude	Phase	Magnitude	Phase
Center of inner conductor	0.03	0.00	0.00	0.00
Edge of inner conductor	3.62	0.02	4.50	1.88
Between both conductors	0.06	0.00	0.00	0.07
Inner edge of outer cond.	0.15	0.01	0.10	0.33
Center of outer conductor	0.03	0.00	0.10	0.00
Outer edge of outer cond.	0.21	0.01	0.10	1.17

TABLE II
PERCENTAGE CHANGE IN THE MAGNITUDE AND PHASE OF THE INPUT IMPEDANCE DUE TO SURFACE ROUGHNESS (ON THE ORDER OF 0.2 × 0.2 MM^2) ON THE INPUT IMPEDANCE OF A LOW-LOSS MATERIAL Al_2O_3 AND A HIGH-LOSS MATERIAL SiC

Placement of surface roughness aberration:	Al_2O_3		SiC	
	Magnitude	Phase	Magnitude	Phase
Center of inner conductor	0.03	0.00	0.10	0.04
Edge of inner conductor	9.46	0.06	12.46	5.04
Between both conductors	0.27	0.00	0.10	0.33
Inner edge of outer cond.	0.80	0.08	0.21	2.45
Center of outer conductor	0.06	0.00	0.10	0.07
Outer edge of outer cond.	0.53	0.03	0.21	3.12

inner conductor. In all cases, the effect of the surface roughness on the phase of the input impedance is rather small.

C. Thin-Sample Measurements

To make thin-sample dielectric properties measurements, thin samples of various thicknesses and complex permittivities were modeled using the FDTD code. The input impedances were then graphed versus complex-permittivity values for different thicknesses and frequencies. To help standardize the measurement procedure, all samples are backed with a standard material such as a highly conducting metal plate. The impedance of the desired sample (backed with the standard material) is then measured with the open-ended probe using a vector network analyzer. The measured impedances are then compared with the FDTD graphs and the values of the complex permittivity, as a function of frequency, are obtained through interpolation.

1) Room-Temperature Measurements: Two different samples, a 5-mm-thick Teflon and a 2.5-mm-thick ZrO_2+ 8 mol% Y_2O_3, were measured using this method to determine the validity of the developed analysis procedure. In both cases, the samples were modeled and measured using both a highly conducting plane (metal) and air as the standard material. The dielectric constant of Teflon is generally known to be about $\epsilon_r' = 2.1$ [15]. The value for ϵ_r'', though not generally agreed upon, is expected to be extremely small and of the order of 10^{-4}. Therefore, when modeling Teflon a value of $\epsilon_r^* = 2.1 - j0$ was used in the FDTD modeling and calculations. For the analysis, 5-mm samples with ϵ_r' values of 1.5, 2.1, and 3 were modeled (with both a metal backing and an air backing) over the frequency range from 500 MHz to 3 GHz in steps of 100 MHz.

The ZrO_2 was measured using cavity-perturbation methods and was found to have the complex-permittivity value of $\epsilon_r^* = 17.9 - j0.02$ [16]. For low-loss materials, changing small ϵ_r'' values such as from 0.02 to 0.03 causes only negligible differences in the FDTD simulated impedance values. This implies that this method can be used with only a rough estimate of the loss factor of the material under test, provided that the material is a low-loss material, which is generally true of ceramic substrates used in the semiconductor industry. Therefore, 2.5-mm-thick samples with $\epsilon_r'' = 0.02$ and $\epsilon_r' = 15$, 18, and 20 were modeled, once again (with both a metal backing and an air backing) over the frequency range from 500 MHz to 3 GHz in steps of 100 MHz. Fig. 12 shows the results of the FDTD modeling of 5-mm-thick samples with various values of the dielectric constant ϵ_r'. Fig. 12(a) shows the metal-backed results, while Fig. 12(b) shows the air-backed input-impedance results. Fig. 13 shows the results of the FDTD modeling of 2.5-mm-thick samples with various values of the dielectric constant ϵ_r'. Fig. 13(a) shows the metal-backed results, while Fig. 13(b) shows the air-backed input-impedance results.

The impedance values of the Teflon and ZrO_2 samples were measured over the frequency range of 500 MHz to 3 GHz using the metallized-ceramic probe. Once again, the samples were measured with both a metal and an air backing. Figs. 14 and 15 show the measured results that have been superimposed on the calculated FDTD impedance values.

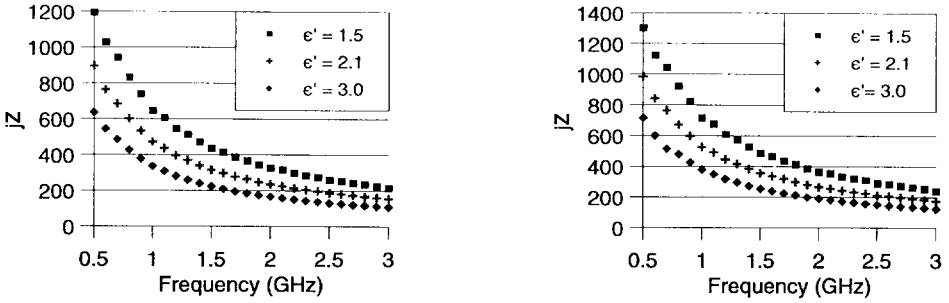

(a) (b)

Fig. 12. The FDTD numerical simulation results of a 5-mm-thick sample with various dielectric constants with (a) sample backed with metal and (b) sample backed with air. The input impedance of the probe is shown versus frequency over the frequency range from 500 MHz to 3 GHz. Dielectric constant of the material under test is obtained through interpolation.

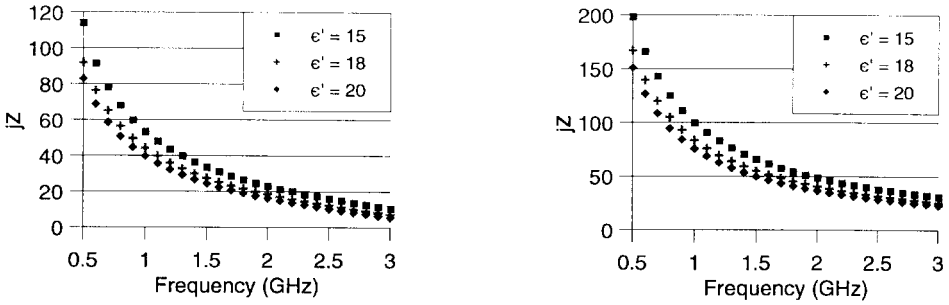

(a) (b)

Fig. 13. The FDTD numerical simulation results of a 2.5-mm-thick sample with various dielectric constants with (a) sample backed with metal and (b) sample backed with air. The input impedance of the probe is shown versus frequency over the frequency range from 500 MHz to 3 GHz.

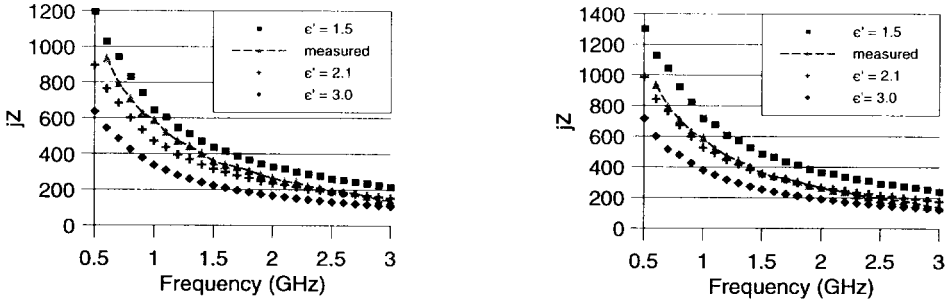

(a) (b)

Fig. 14. Measured results of a 5-mm-thick sample of Teflon with (a) sample backed with metal and (b) sample backed with air, superimposed over the FDTD simulation results shown in Fig. 12. Results are shown over the frequency range from 500 MHz to 3 GHz.

By interpolating the experimentally measured impedance results with the FDTD calculated results, the dielectric constant of both the Teflon and the ZrO_2 were calculated. Fig. 16 shows the ϵ_r' results for Teflon compared to the literature values, and Fig. 17 shows the ϵ_r' results for ZrO_2 compared to values from measurements using the cavity perturbation technique.

Upon analyzing the results from these measurements, it was found that the worst-case error for the ZrO_2 results were about 8%. These results show that the developed procedure will provide valid and accurate complex-permittivity results.

2) High-Temperature Measurements: With the developed knowledge obtained from the high-temperature error analysis, as well as the newly developed thin-sample measurement technique, it was decided to extend the measurement of thin samples to high temperatures. Two different ceramic substrates used in making microwave circuits were measured at temperatures up to 800 °C. The substrates measured were alumina and sapphire, with both of the substrates being measured at 0.6 mm thick. The same procedure as explained in the previous section was used, and the sample was backed with air.

Figs. 18 and 19 show the interpolated values of the dielectric constant of both alumina and sapphire as compared to values obtained using cavity perturbation techniques. Fig. 18 shows the results at 600 °C, and Fig. 19 shows the results at 800 °C. Using cavity techniques, the value of the dielectric constant ϵ_r' of alumina is $\epsilon_r' = 10.38$ at 600 °C, and $\epsilon_r' = 11.18$ at 800 °C. The value of the dielectric constant ϵ_r' of sapphire is $\epsilon_r' = 11.00$ at 600 °C, and $\epsilon_r' = 12.34$ at 800 °C. It is shown in Figs. 18 and 19 that there is good agreement between the newly developed method for thin-sample measurements

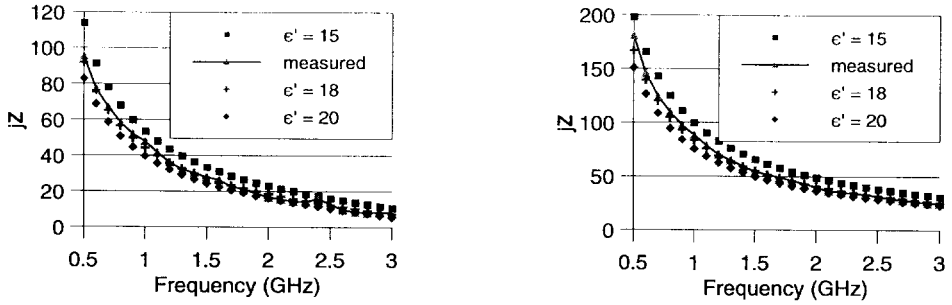

(a) (b)

Fig. 15. Measured results of a 2.5-mm-thick sample of ZrO_2 + 8 mol% Y_2O_3 with (a) sample backed with metal and (b) sample backed with air, superimposed over the FDTD simulation results shown in Fig. 13. Results are shown over the frequency range from 500 MHz to 3 GHz.

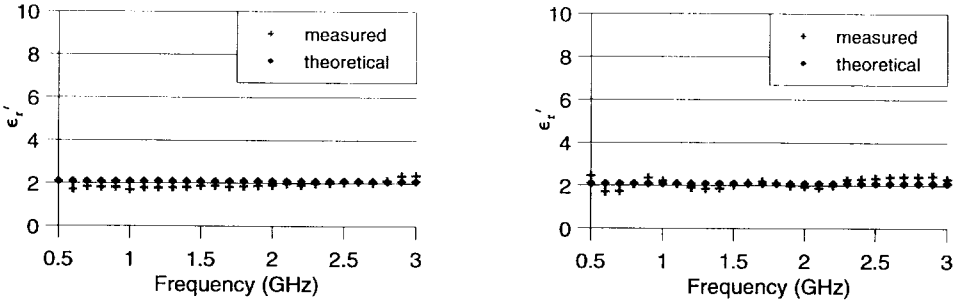

(a) (b)

Fig. 16. Measured results of a 5-mm-thick sample of Teflon with (a) sample backed with metal and (b) sample backed with air, compared to values from literature. Results are shown over the frequency range from 500 MHz to 3 GHz.

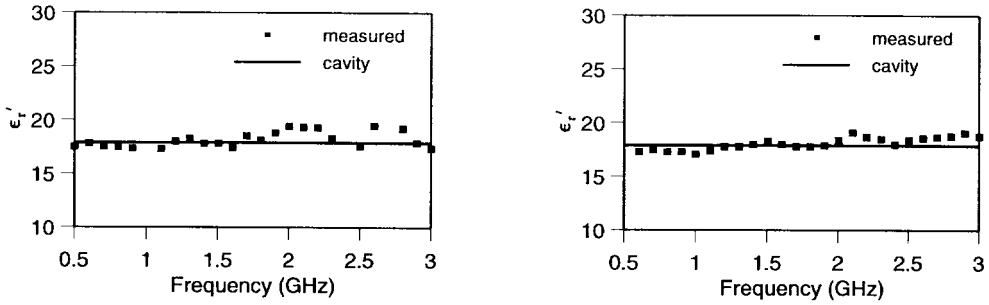

(a) (b)

Fig. 17. Measured results of a 2.5-mm-thick sample of ZrO_2 + 8 mol% Y_2O_3 with (a) sample backed with metal and (b) sample backed with air. Results are compared with values from perturbation techniques.

using FDTD numerical simulations and results from the cavity perturbation technique.

II. Conclusions

New aspects of the development and utilization of a metallized-ceramic probe were investigated in this paper. First, an uncertainty analysis was performed to quantify the errors due to the differential thermal expansion between the inner and outer conductors of the metal coaxial probes. It was determined that an air gap as small as 0.1 mm between the inner conductor and the material under test can cause errors as high as 170% in the measured input impedance, and can even cause errors as high as 50% in low-loss materials. To assist in the numerical modeling of air gaps on the order of 0.1 mm, a 2-D cylindrical FDTD code was developed and used. The 2-D code was validated by comparison with analytical results published in [14] for the special case when an air gap exists between the coaxial probe and the sample under test. Another error analysis was completed to quantify the effect of surface roughness on the measured input impedance of the sample under test. It was determined that surface roughness has negligible effect unless the roughness aberration just happens to be below the edge of either the inner or outer conductor. This type of measurement error may, hence, be overcome by repeating the measurements at different locations on the sample and then averaging the obtained results.

A second new aspect of the developed metallized-ceramic probe is related to the use of FDTD numerical simulations to make dielectric properties measurements of electrically "thin" samples. By backing the material under test with a

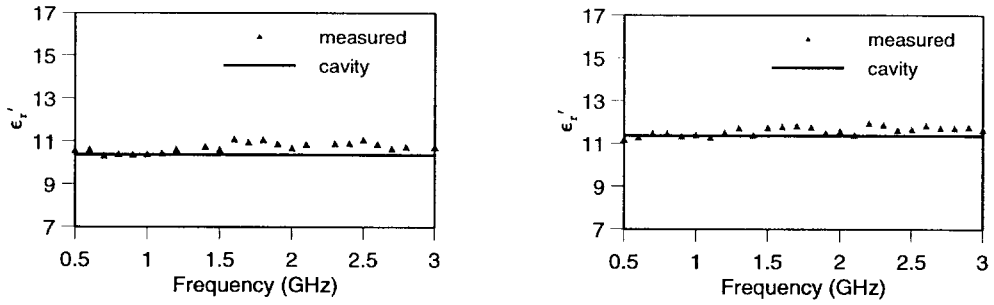

Fig. 18. Measured results of a 0.6-mm thin sample of (a) alumina and (b) sapphire at 600 °C. Results are compared with values from cavity perturbation techniques.

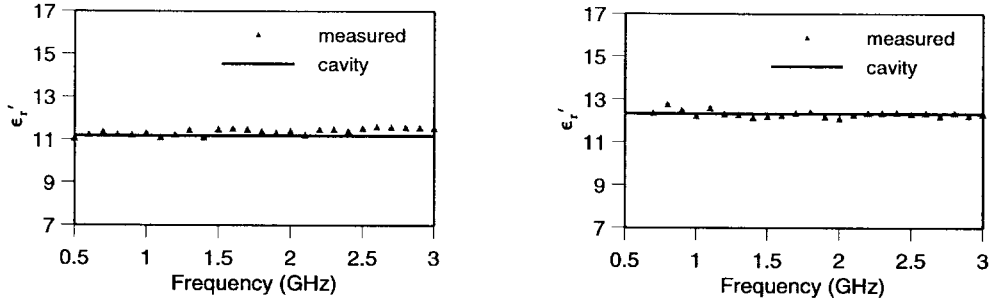

Fig. 19. Measured results of a 0.6-mm thin sample of (a) alumina and (b) sapphire at 800 °C. Results are compared with values from cavity perturbation techniques.

standard material such as a conducting plate or air, the complex permittivity of thin samples can be accurately measured. A 5-mm-thick sample of Teflon as well as a 2.5-mm-thick sample of ZrO_2 were accurately measured using the developed method. Another new aspect related to the use of the probe is the extension of the thin-sample measurements to high temperatures. A 0.6-mm substrate of alumina and sapphire were measured at temperatures as high as 800 °C. These materials are both used in the production of microwave integrated circuits. Therefore, this newly developed method has important applications in on-line wafer characterization in the semiconductor and microwave integrated-circuit industries.

ACKNOWLEDGMENT

The authors are indebted to the reviewers whose comments and suggestions were thoughtful and constructive and, hence, contributed to the value of this paper.

REFERENCES

[1] S. Bringhurst and M. F. Iskander, "Open-ended metallized ceramic coaxial probe for high temperature dielectric properties measurements," *IEEE Trans. Microwave Theory. Tech.*, vol. 44, pp. 926–935, June 1996.

[2] E. C. Burdette, F. L. Cain, and J. Seals, "*In vivo* probe measurement technique for determining dielectric properties at VHF through microwave frequencies," *IEEE Trans. Microwave Theory. Tech.*, vol. MTT-28, pp. 414–427, Apr. 1980.

[3] E. Tanabe and W. T. Joines, "A nondestructive method for measuring the complex permittivity of dielectric materials at microwave frequencies using an open transmission line resonator," *IEEE Trans. Instrum. Meas.*, vol. IM-25, pp. 222–226, Sept, 1976.

[4] D. Misra *et al.*, "Noninvasive electrical characterization of materials at microwave frequencies using an open-ended coaxial line: Test of an improved calibration technique," *IEEE Trans. Microwave Theory. Tech.*, vol. 38, pp. 8–14, Jan. 1990.

[5] O. M. Andrade, M. F. Iskander, and S. Bringhurst, "High temperature broadband dielectric properties measurement techniques," *Microwave Processing of Materials III* (Materials Res. Soc.), vol. 269, pp. 527–539, 1992.

[6] D. Blackham, "Calibration method for open-ended coaxial probe/vector network analyzer system," *Microwave Processing of Materials III* (Materials Res. Soc.), vol. 269, pp. 595–599, 1992.

[7] M. F. Iskander and J. B. Dubow, "Time- and frequency-domain techniques for measuring the dielectric properties of rocks: A review," *J. Microwave Power*, vol. 18, pp. 55–74, 1983.

[8] C. L. Li and K. M. Chen, "Determination of electromagnetic properties of materials using flanged open-ended coaxial probe—Full-wave analysis," *IEEE Trans. Instrum. Meas.*, vol. 44, pp. 19–27, Feb. 1995.

[9] P. De Langhe, K. Blomme, L. Martens, and D. De Zutter, "Measurement of low-permittivity materials based on a spectral-domain analysis for the open-ended coaxial probe," *IEEE Trans. Instrum. Meas.*, vol. 42, pp. 879–886, Oct. 1993.

[10] K. S. Yee, "Numerical solution of initial boundary-value problems involving Maxwell's equations in isotropic media," *IEEE Trans. Antennas Propagat.*, vol. AP-14, pp. 302–307, May 1966.

[11] S. Bringhurst, M. F. Iskander, and P. Gartside, "FDTD simulation of an open-ended metallized ceramic probe for broadband high-temperature dielectric properties measurements," in *Appl. Computational Electromagnetics, ACES Conf. Proc.*, vol. I, Monterey, CA, Mar. 1994, pp. 473–477.

[12] F. P. Beer and E. R. Johnston, *Mechanics of Materials*, 2nd ed. New York: McGraw Hill, 1992, p. 64.

[13] W. H. Kohl, *Materials and Techniques for Electron Tubes, General Telephone and Electronics Technical Series.* New York: Reinhold, 1960.

[14] J. Baker-Jarvis, M. D. Janezic, P. D. Domich, and R. G. Geyer, "Analysis of an open-ended coaxial probe with lift-off for nondestructive testing," *IEEE Trans. Instrum. Meas.*, vol. 43, pp. 711–718, Oct. 1994.

[15] C. A. Balanis, *Advanced Engineering Electromagnetics.* New York: Wiley, 1989, p. 79.

[16] S. Bringhurst, M. F. Iskander, and O. M. Andrade, "High-temperature dielectric properties measurements of ceramics," *Microwave Processing of Materials III* (Materials Res. Soc.), vol. 269, pp. 561–568, 1992.

Shane Bringhurst (S'93–M'96) received the B.S., M.S., and Ph.D. degrees in electrical engineering from the University of Utah, Salt Lake City, in 1992, 1995, and 1996, respectively.

He has worked as both a Research and Teaching Assistant at the University of Utah. In 1996, he joined the Antenna/Nonmetallic Department, Texas Instruments, Incorporated, McKinney, TX, where he is working with the Computational Electromagnetics Group in antenna design. His research interests have included dielectric properties measurements, microwave sintering of ceramics, microwave and RF drying of ceramics, and numerical techniques in electromagnetics.

Magdy F. Iskander (S'72–M'76–SM'84–F'93) is Professor of electrical engineering at the University of Utah, Salt Lake City, Director of the NSF/IEEE Center for Computer Applications in Engineering Education (CAEME), and Director of the State Center of Excellence for Multimedia Education and Technology. In 1986, he established the Engineering Clinic Program to attract industrial support for projects to be performed by engineering students at the University of Utah. Since then, over 80 projects have been sponsored by 26 corporations from across the United States. He is also the Director of the Conceptual Learning of Science (CoLoS) USA Consortium, which is sponsored by the Hewlett-Packard Company and has 11 member universities across the United States. He authored the textbook *Electromagnetic Fields and Waves,* (Prentice-Hall, 1992), and has edited the *CAEME Software Book,* vol. I (1991) and vol. II (1994), and four other books on *Microwave Processing of Materials,* (Materials Research Society, 1990, 1992, 1994, 1996). He edited two special issues of the *Journal of Microwave Power,* (March 1983 and September 1983). He has also edited a special issue of the *ACES Journal* on computer-aided electromagnetics education and the proceedings of both the 1995 and 1996 International Conferences on Simulation and Multimedia in Engineering Education. He has published over 150 papers in technical journals and has made numerous presentations in technical conferences.

Dr. Iskander is a member of the National Research Council Committee on Microwave Processing of Materials. He is a distinguished lecturer for the IEEE Antennas and Propagation Society. He is the Editor of *Computer Applications in Engineering Education, (CAE),* (Wiley). an associate editor of the IEEE TRANSACTIONS ON ANTENNAS AND PROPAGATION, and an Associate Editor of the IEEE AP-S Magazine. He has received the Curtis W. McGraw ASEE National Research Award for outstanding early achievements, the ASEE George Westinghouse National Award for innovation in engineering education, and the 1992 Richard R. Stoddard Award from the IEEE Electromagnetic Compatability (EMC) Society.

Mikel J White was born in Milford, UT, on May 29, 1969. He received the B.S. (*magna cum laude*), M.S., and Ph.D. degrees in electrical engineering from the University of Utah, Salt Lake City, in 1992, 1996, and 1997, respectively.

He is currently with Texas Instruments, Incorporated, Dallas, TX. He has published papers on numerical modeling of electrically large objects and multimode microwave systems using the FDTD method, and has made several presentations at international conferences.